Morphological description of microplastic particles for environmental fate studies

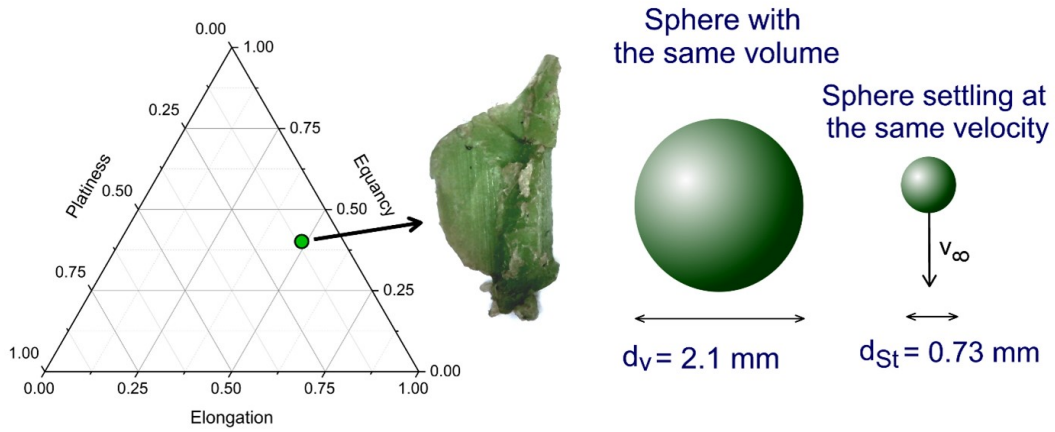

Morphological description of microplastic particles for environmental fate studies

Roberto Rosal*

Department of Chemical Engineering, Universidad de Alcalá, E-28871 Alcalá de Henares, Madrid, Spain

Abstract

The morphological description of microplastic particles is mostly based on subjective descriptors. However, data intercomparison require unambiguous classifications. This work presents a morphological description based on the lengths of the smallest enclosing orthogonal parallelepiped. Three dimensionless parameters, namely equancy, platiness and elongation describe any particle shape with reference on the basic 3D (sphere), 2D (plate) and 1D (rod) shapes. The particle size directly linked to the environmental fate of microplastics is the Stoke's diameter. The derivation of Stoke's diameter based on 3D morphological descriptors is explained and the proxies that can be used if only 2D projected images are available is discussed. This work shows that the behaviour of irregular particles is not adequately predicted using as descriptor the diameter of the sphere with the same volume as the particle. There is a need to obtain equations specifically developed for plastic particles, especially for fibres, and for the atmospheric compartment.

1. Introduction

The pollution due to plastic waste is an emerging global issue. Initially identified in marine ecosystems, the presence of plastic litter has already been acknowledged in the most diverse environments (González-Pleiter et al., 2021; Obbard, 2018; Wang et al., 2020). Besides their composition, based on synthetic polymers, size is the main parameter used to classify plastic debris because it is the main factor determining their mobility in fluid media and their interaction with the biota. However, size is a property difficult to unambiguously define except for the case of regular particles. Small plastic particles are defined as microplastics (MPs) if their larger dimension is < 5 mm. This cut-off is rather arbitrary and up to a certain extent contradictory with the prefix "micro", but the term has become a well-established standard. The UN advisory Group of Experts on the Scientific Aspects of Marine Environmental Protection (GESAMP) recommended the inclusion of all particles < 5 mm for the assessment of sources, fate and effects of microplastics to preserve the information provided by the many studies published so far with that cut-off (GESAMP, 2015, 2016). GESAMP also specified that if particles depart significantly from sphericity, the 5 mm boundary (and by analogy all references to "size") should refer to the largest dimension (GESAMP, 2019). The lower boundary of MPs is usually taken as 1 µm, below which, the particles would be considered nanoplastics (NPs). That cutoff is also controversial as it is in conflict with the prefix "nano" used for engineered nanoparticles with at least one dimension < 100 nm and with the recent ECHA's Background Document proposing restrictions to intentionally added microplastics (ECHA, 2020).

The fate and effects of MPs and NPs depend on their size, but also on their shape. The dispersion of plastic particles in aquatic and atmospheric environments is critically related to particle-fluid interaction, which determines their settling or buoyancy. The existing data showed that particle shape strongly influences the behaviour of plastic particles in fluid media and, therefore, important discrepancies exist between experimental settling or rising velocities and the values predicted from models assuming spherical geometry (Khatmullina and Isachenko, 2017; Kowalski et al., 2016). The behaviour of MPs in fluids is not an easy problem. MPs sizes span over three orders of magnitude (equivalent to the difference between a garden ant and a blue whale) and plastic shapes are very variable and sometimes quite different from simple geometries. MP shapes include one-dimensional fibres, two-dimensional films and a large variety or fragments, either primary, specifically produced in the microplastics size range, or secondary, consequence of the ageing and fragmentation of larger particles. Another difficulty is that the colonization of MPs by microorganisms influences their fate by changing particle density. Some results showed that biofilm growth tend to increase the density of the plastic particles favouring their tendency to sink in water (Semcesen and Wells, 2021). Besides, the properties of the receiving environment such as

* Corresponding author: roberto.rosal@uah.es
Available online: July 14, 2021

water salinity and temperature, air density, currents and winds can fluctuate greatly and in such complex environments, particle shape is an important factor (Forsberg et al., 2020). Finally, it has been shown that the behaviour of the smaller plastic particles depend on their heteroaggregation with suspended solids which is a process particularly difficult to model (Besseling et al., 2017).

A major issue in the research about plastic waste is the difficulty to compare concentration data among different studies. Plastic concentration is expressed by some authors as items per unit of volume or weight of the environmental matrix, while others express concentration as weight of plastic per weight or volume of the environmental matrix (Vighi et al., 2021). The surface area of plastic debris has also been used to describe the abundance of plastic in natural environments (Rivers et al., 2019). The incomplete characterization of particles makes it very difficult to compare data reported in different units and complicates risk assessment and the possible inclusion of MPs and NPs in regulatory frameworks. Surface area, weight and number are not easy to compare in the absence of a full characterization of particle morphology, which is a complex task seldom performed in environmental studies of plastic debris. In most cases, shape and size characterization of MPs is based on projected microscopy images, making it difficult to derive all relevant morphological information required for a correct risk assessment (Gray and Weinstein, 2017). It is interesting to point out that the software commonly used in FTIR or Raman microscopes can perform particle recognition determining size and shape by automatic image processing, thereby offering the possibility of combining spectroscopic information with particle features (Brandt et al., 2020; Cowger et al., 2020). MPs also present differences in surface roughness, which is a parameter closely related to the embrittlement and fragmentation of particles and with their microbial colonization (Lusher et al., 2020). However, concerning the behaviour of plastics in fluid media, the role of surface roughness is usually negligible at low or intermediate Reynolds numbers, which are those expected for plastics in the environment (Bagheri et al., 2015).

This study presents a characterization of plastic particles based on three parameters namely, equancy, platiness and elongation suitable for representation in a ternary diagram. The derivation of equivalent diameters is discussed including Stoke's diameter, which is the most relevant in terms of buoyancy or settling behaviour. Methods are provided to obtain estimations of particle volume and surface, which are important for calculating particle-fluid interactions. Knowledge gaps and research priorities on plastic-fluid interaction are presented including the limitations associated to the use of particle descriptors based on 2D images.

2. Shape and size of microplastic particles

MPs are very heterogeneous, displaying a wide variety of shapes that range from regular spherical or cylindrical pellets to fibres with high aspect ratio. Once in the environment, plastic materials suffer physiochemical degradation processes that lead to the disintegration or larger particles into smaller irregular fragments. The identification of the different morphologies of the MPs found in environmental samples is a customary way of providing some classification based on properties easy to derive without the need of sophisticated instruments. Besides, morphological identification provides hints on the sources of plastic pollution and information about the fate of a particular type of debris. This is the case of fibres from synthetic textiles, rests of fishing gears, industrial pellets and many more. However, the unambiguous identification of heterogeneous three-dimensional objects is a difficult task. Table 1 summarizes some recent categories found in the literature for the morphological categorization of MPs.

In many cases, the use of certain names hints towards the origin of the particles. Beads allude to the use of primary MPs in cosmetics. Pellets are usually associated to plastic manufacturing. Fragments have been defined as particles with irregular shape and edges, suggesting an origin in the fragmentation of larger particles, although this is not necessarily true (Hartmann et al., 2019). Foams evoke foamed polystyrene, expanded or extruded (sometimes erroneously put together under the tradename styrofoam), although other foamed plastics exist in the market. Films are also irregular, but thinner than fragments and possibly flexible. Sharp ends and the same thickness along their length has been used to distinguish filaments from fibres, but the difference is rather arbitrary (Magni et al., 2019). Sometimes "moulded particles" are included as subcategory of plastic fragments that did not completely lose their original shape (Edo et al., 2019; Hidalgo-Ruz et al., 2012). GESAMP recommends five main morphological categories, namely fragments, foams, films, lines, and pellets. The category 'lines' is based on the aspect ratio of the particles and include filaments and fibres (GESAMP, 2019). Such morphological descriptors have been proposed to allow harmonization and comparison among data from different sources and campaigns. However, they entail a considerable

Table 1. *Commonly reported types of microplastics by morphology.*

Categories	Number of categories	Reference
Fragments, pellets, filaments, films, foamed plastic, granules, and styrofoam	7	(Hidalgo-Ruz et al., 2012)
Pellets, fragments, fibres, films, ropes and filaments, microbeads, sponges/foams, and rubber	8	(Frias et al., 2018)
Beads-spherules, foams, films, fragments, and fibres	5	(Burns and Boxall, 2018)
Spheres, spheroids, rod-shaped plastics, fragments, films, and fibres	6	(Hartmann et al., 2019)
Fibres, lines, films, and fragments	4	(Magni et al., 2019)
Fragments, pellets, moulded particles, foams, filaments, microbeads, and films	7	(Edo et al., 2019)
Fragments, foams, films, lines, and pellets	5	(GESAMP, 2019)
pellets, fragments, fibres, (films, ropes, filaments, sponges, foams, rubber, and microbeads)*	10	(Frias and Nash, 2019)
Fragments, films, fibres, and filaments	4	(Edo et al., 2021)

* Less abundant and in decreasing order, according to the authors.

degree of subjectivity, which make them of limited usefulness.

Different quantitative descriptors have been used to characterize particle shape. The main linear dimensions, length, width, and height provide a basic characterization of particle shape, but there are other descriptors like roundness and irregularity, which can be obtained from image processing (Blott and Pye, 2008). Roundness refers to the presence of corners and edges whereas irregularity relates to the deviation from a regular three-dimensional body due to the presence of concavities and convexities. In practice, the behaviour of particles in fluid media essentially depends on their main dimensions, unevenness and surface irregularities playing a minor role (Khatmullina and Isachenko, 2017). The settling or buoyancy behaviour of particles are generally based on correlations developed for regular or near-to-regular shapes, which drives to the difficult problem of obtaining valid shape descriptors. Recently, the techniques of 3D laser range scanner and X-ray microtomography (X-ray mCT) allowed obtaining information on 3D particle shape in relatively short time (Lin and Miller, 2005). X-ray mCT builds a 3D array of elemental digital units called voxels from 2D projections acquired during tomographic scanning (Bozzini et al., 2018). The volume and surface of each particle are measured by adding the volume of all individual voxels and their external area respectively. In practice, the calculation of particle length, width, and height, reduces to solving an eigenvalue problem for inertia matrix (Safonov et al., 2018). Incidentally, a method exist that provides analytical functions of the external surface of 3D particles by combining X-ray mCT and spherical harmonic analysis (Garboczi and Bullard, 2017). Although still of limited use X-ray mCT has already been used for MPs research (Sagawa et al., 2018; Tötzke et al., 2021).

The parametrization of particle shape requires the determination of its three main orthogonal dimensions, namely length, width and height or L (longest), I (intermediate or longest dimension perpendicular to L) and S (smaller or the dimension perpendicular to L and I). The determination of the three orthogonal dimensions is not always unambiguous, but for the sake of clarity, they can be defined as the lengths of the smallest orthogonal parallelepiped enclosing the particle (Blott and Pye, 2008). It is not easy to ensure that an enclosing parallelepiped is the smallest one, but in most cases, the differences should be minor. The three orthogonal dimensions defining particle shape and size can be ascribed to the axes of an ellipsoid (Merikallio et al., 2015). Fig. 1 shows the projection of a MP particle on three orthogonal planes, its enclosing parallelepiped, and the ellipsoid with the same orthogonal dimensions or "equivalent" ellipsoid.

The modeling of particles using ellipsoids has some limitations in the case of highly polygonal particles or irregular objects but can be assumed as a reasonable way of dealing with the large sets of heterogeneous particles obtained from environmental samples. The fitting is better for convex particles, which are those for which any point in the segment joining two points of the particle also belong to the particle. Few particles encountered in natural and industrial environments are convex, but a class of non-convex particles called star-shaped particles can be reasonably described by ellipsoids. A particle is star-shaped if there exists a point inside it from which a line joining any other point falls entirely inside the particle (Garboczi and Bullard, 2017). (Note that the

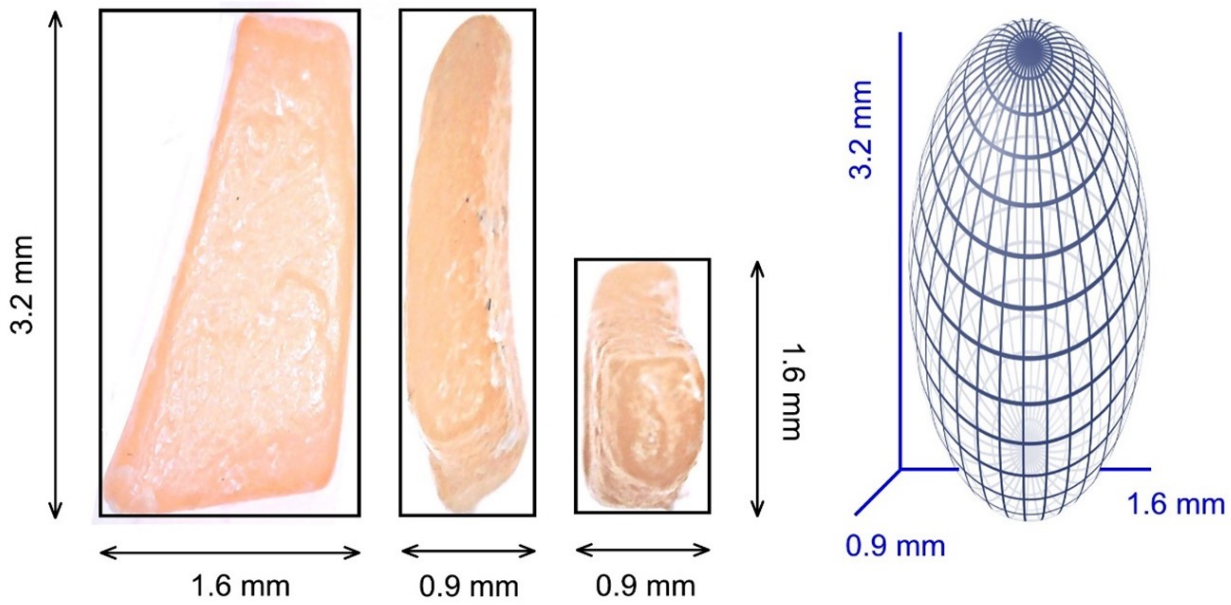

Figure 1: *Microplastic particle defined by the lengths of the smallest enclosing orthogonal parallelepiped and ellipsoid with the same orthogonal dimensions as axes.*

particle of Fig. 1 is not strictly convex.) If a particle can be described by an ellipsoid, its volume can be easily computed as that of the ellipsoid. The volume of a general (scalene or triaxial) ellipsoid with axes d_1, d_2 and d_3 ($d_1 > d_2 > d_3$) is:

$$V = \frac{\pi\, d_1\, d_2\, d_3}{6} \tag{1}$$

If $d_1 \approx d_2 \gg d_3$, the ellipsoid is oblate (flat); if $d_1 \gg d_2 \approx d_3$ the ellipsoid is prolate (sharp, like the one shown in Fig. 1). From the main orthogonal dimensions, a mean size (d_{3D} or geometric diameter), can be defined as follows:

$$d_{3D} = \frac{d_1 + d_2 + d_3}{3} \tag{2}$$

Other descriptors based on the main orthogonal dimensions, such as 3D aspect ratio (AR_{3D}) are also immediate (note that $AR_{3D} > 1$ as defined here):

$$AR_{3D} = \frac{1}{2}\left(\frac{d_1}{d_2} + \frac{d_2}{d_3}\right) \tag{3}$$

Other shape factor widely used to measure particle flattening is the Corey's shape factor defined as the ratio of the length of the shortest dimensions to the geometrical mean of the other two axes:

$$csf = \sqrt{\frac{d_3^2}{d_1\, d_2}} \tag{4}$$

The approximation of arbitrary particles to scalene ellipsoids allows computing their external surface, S, using d_1, d_2, d_3, and the following expression, known as Knud Thomsen's formula, in which p is an empirical parameter:

$$S \backsimeq 4\,\pi\, 3^{-\frac{1}{p}} \left[\left(\frac{d_1}{2}\right)^p \left(\frac{d_2}{2}\right)^p + \left(\frac{d_1}{2}\right)^p \left(\frac{d_3}{2}\right)^p + \left(\frac{d_1}{2}\right)^p \left(\frac{d_3}{2}\right)^p\right]^{\frac{1}{p}} \tag{5}$$

Using p = 1.6075, the error of Eq. 5 is generally below 1 % (Ulanovsky and Pröhl, 2006). The reason to use an approximate expression like Eq. 5 is that the analytical derivation of the surface area is rather complicated. The exact solution, that involves elliptic integrals, can be found elsewhere (Keller, 1979).

The three main orthogonal dimensions, d_1, d_2, d_3, (L, I, and S in other works) can be used to quantify particle shape. If all dimensions are approximately equal, the particle is close to spheric (isometric), but the same happens if d_3/d_1 is close to the unity, and, therefore, that ratio has been proposed to measure *equancy* (Szabó and Domokos, 2010). The *platiness* of the particle is given by the discrepancy between the minor dimension and the other two, which can be measured by (d_2 - d_3)/d_1. In rod-shaped particles, one dimension is significantly larger than the other two, and, therefore (1 - d_2/d_1) can be used as a measure of particle *elongation*.

$$equancy = \frac{d_3}{d_1} \tag{6}$$

$$platiness = \frac{d_2 - d_3}{d_1} \tag{7}$$

$$elongation = 1 - \frac{d_2}{d_1} \tag{8}$$

Clearly, the sum of these three parameters is the unity:

$$\left(\frac{d_3}{d_1}\right) + \left(\frac{d_2 - d_3}{d_1}\right) + \left(1 - \frac{d_2}{d_1}\right) = 1 \tag{9}$$

Other ways of defining form factors can be found elsewhere (Blott and Pye, 2008). However, the three ratios mentioned before are particularly convenient to represent particles in a barycentric triangular plot, with isolines parallel to triangle sides and having as vertexes the three basic shapes:

3D: spheres, spheroids (near spherical shape) or fragments (irregular shape). *2D*: plates, films flaked particles with relatively flat surface. *1D*: fibres and rod-shaped high aspect ratio cylindrical objects.

The three basic morphologies together with a set of plastic particles sampled from marine litter are represented in Fig. 2 in a ternary plot with axes representing equancy, platiness, and elongation. Details are given in Table S1 (Supplementary Material, SM). The selected particles were measured and photographed using a stereomicroscope by fixing the particles to a transparent scaffold, which allowed taking pictures of two dimensions over a stable position as well as images over the perpendicular plane. ImageJ, a widely used public domain Java-based image processing software developed by the USA National Institutes of Health, was used to process the images. It is important to note that the three orthogonal dimensions describing particle size and shape do not change with time. In other words, the description provided here is limited to rigid bodies. In nature there are also flexible bodies, the shape of which can change upon the drag exerted by a moving fluid. In the field of microplastic research, this effect is probably important for fibres, but the behaviour of elastohydrodynamic systems in which flexible bodies change their configuration during flow is very complex and its application to environmental issues still unclear (LaGrone et al., 2019).

3. Equivalent diameter and sphericity

In most cases, it is desirable to assign one single length dimension to a given particle irrespective of its geometrical complexity. 'Equivalent' diameters are generally defined by linking one particle size-dependent property with the same property of a spherical particle, the diameter of which gives the equivalence in terms of that particular property. An immediate one is sieve diameter, defined as the diameter of a sphere passing through the same opening, but although widely used, the information provided by mesh opening size is limited. The most widely used equivalent diameter is that of the sphere with the same volume as the particle, d_v:

$$d_v = \left(\frac{6V}{\pi}\right)^{\frac{1}{3}} \tag{10}$$

Other equivalent diameters used sometimes are those of the sphere with the same surface, d_s, and the sphere with the same surface-to-volume ratio or Sauter's diameter. The latter is important for applications in which the specific area of the solid is important, but for the sedimentation (or flotation) of particles in a fluid, volume equivalent diameter is the most relevant particle size.

The comparison of a particle shape to the equivalent sphere is usually given as the ratio of the surface area of a sphere with the same volume (as the particle) to the surface area of the particle, S. This is a non-dimensional parameter called sphericity, ϕ which is the unity for a perfect sphere and < 1 for the rest of geometries:

$$\phi = \frac{\sqrt[3]{36\pi V^2}}{S} = \frac{\pi d_v^2}{S} \tag{11}$$

Fig. 3 shows the sphericity of ellipsoids with different combinations of their three orthogonal dimensions. For equancy > 0.20, the particles can be considered approximately isometric, which are those particles for which $\phi > 0.670$ (Haider and Levenspiel, 1989). It is clear comparing Fig. 3 and Fig. 2 that many particles with geometries usually found in plastic litter cannot be considered isometric. This is important to calculate particle-fluid interaction.

Sphericity can be approached by the sphericity of the ellipsoid having the same dimensions. A discussion about the deviations of this approximation with regards to true sphericity (from Eq. 11) can be found elsewhere (Bagheri et al., 2015). The ratio d_v/d_1 has also been used as proxy for the true particle sphericity (Maroof et al., 2020). Another widely used approximation for particle sphericity is the Corey's shape factor as defined in Eq. 4, which is the unity for spheres and take low values for elongated and flat shapes. Computing sphericities from the main orthogonal dimensions offers the advantage of robustness. Sphericities calculated using Eq. 11, although mathematically correct, strongly depend on the accuracy of particle volume and surface. Particle surface is a parameter particularly difficult to estimate and may lead to high uncertainty in calculated sphericities, at times yielding values even higher than the unity.

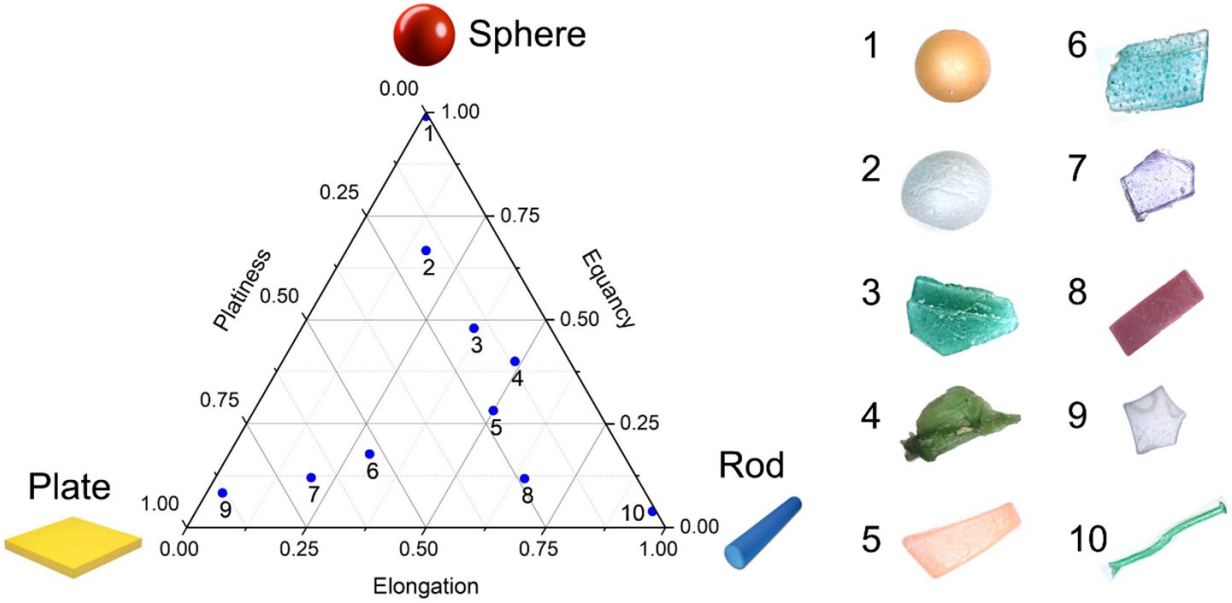

Figure 2: *Basic morphologies for MPs: sphere (3D), plate (2D) and rod (1D) in a ternary plot equancy-platiness-elongation. Numbers 1-10 correspond to real particles sampled from marine litter. Details are given in Table S1 (SM).*

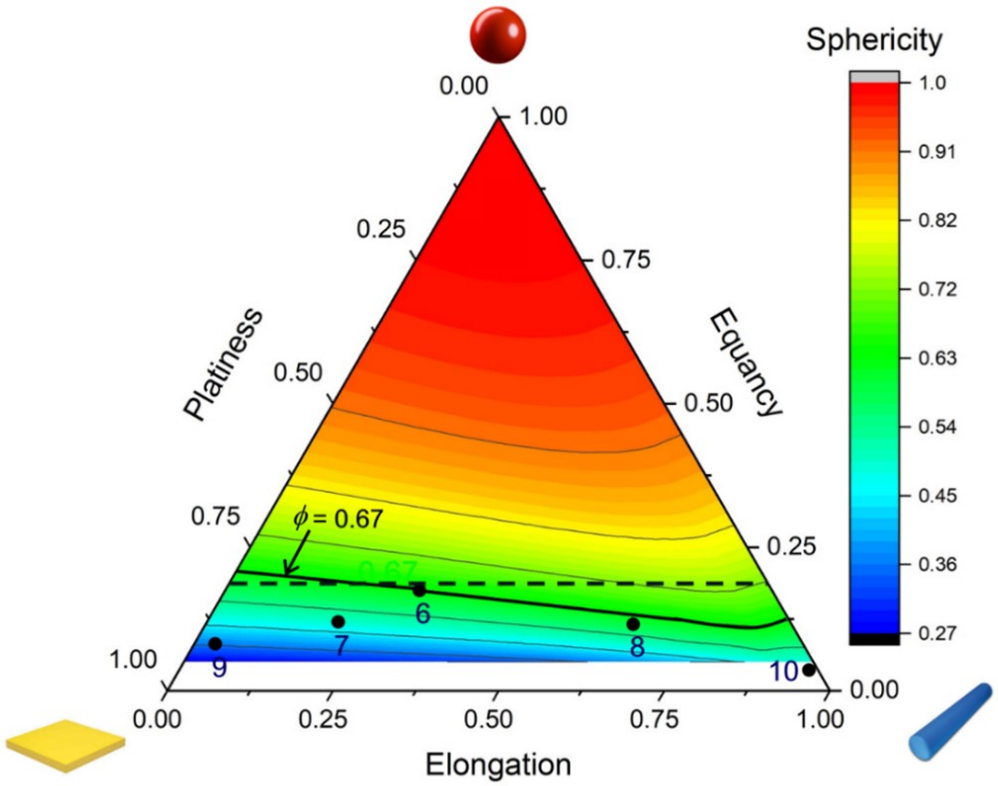

Figure 3: *Sphericity as a function of the parameters describing particle form: Equancy, Platiness and Elongation. Sphericity has been calculated for ellipsoids according to Eqs. 1, 4, 9, and 10. Numbers like in Fig. 2; the dashed line corresponds to equancy 0.20.*

4. Drag coefficient and terminal velocity

For particle sizes > 1 μm, brownian motion is negligible and particle dynamics is only explained by the action of gravity and viscous forces. Incidentally, the colloidal behaviour of such small particles is the main reason for the 1 μm boudary between MPs and NPs (Gigault et al., 2018). All particles immersed in a fluid experience a force in the opposite direction of particle motion, called drag force, F_D, which is proportional to a non-dimensional drag coefficient, c_D, defined by the following expression:

$$F_D \equiv c_D \, S_p \, \frac{1}{2} \, \rho_f \, v_\infty^2 \tag{12}$$

Where v_∞ is the velocity of the particle relative to the fluid, also interpreted as the particle velocity in a quiescent fluid, S_p is the surface projected by the particle on a plane perpendicular to fluid motion, and ρ_f the density of the fluid. In the case of a freely falling (or rising) particle into a stagnant fluid, the balance between the drag force and the gravity leads to the following expression, in which $\Delta\rho$ is the difference in density between particle and fluid (or between fluid and particle), and V is the particle volume:

$$V \, \Delta\rho \, g = c_D \, S_p \, \frac{1}{2} \, \rho_f \, v_\infty^2 \tag{13}$$

Eq. 13 can be solved to obtain the terminal velocity of the particle, provided a value for c_D can be obtained. In the case of spherical particles falling at low velocity, an analytical solution can be derived using the Navier-Stokes equation, yielding the well-known Stoke's equation valid for low Re numbers. The deviations are below 2 % for Re < 0.05, although it is usually accepted for Re < 0.1, which is referred to as Stoke's regime (Happel and Brenner, 2012). For higher Re number, representing for example, higher velocities, several expressions have been developed with the following (or similar) form:

$$c_D = \frac{24}{Re} \left(1 + A Re^B\right) + \frac{C}{1 + \frac{D}{Re}} \tag{14}$$

Haider and Levenspiel proposed a set of values for the empirical parameters A, B, C and D by minimising the root-mean-square differences between calculated and experimental values of the drag coefficient for spherical particles at subcritical (Re < 2.6 x 10^5) incompressible flow: A = 0.1806, B = 0.6459; C = 0.4251 and D = 6880.95 (Haider and Levenspiel, 1989). For the case of non-spherical particles, the parameters A, B, C and D are functions of particle sphericity. Haider and Levenspiel using experimental results from particles with different sphericities proposed the following set of values:

$$A = 8.1716 \, e^{-4.0655\phi} \tag{15}$$

$$B = 0.0964 + 0.5565\phi \tag{16}$$

$$C = 73.69 \, e^{-5.0746\phi} \tag{17}$$

$$D = 5.378 \, e^{+6.2122\,\phi} \tag{18}$$

The approximation of Haider and Levenspiel has been tested for spherical particles at Re < 2.6 x 10^5, non-spherical isometric particles (ϕ < 0.670) at Re < 25000, and disks at Re < 500. Other similar expressions have been proposed with the same rationale and simliar overall accuracy (Clift and Gauvin, 1971). Ganser formulated a generalized expression for c_D as a function of Stoke's and Newton's shape factors, K_1 and K_2 respectively:

$$c_D = \frac{24}{Re \, K_1} \left[1 + A \left(Re \, K_1 \, K_2\right)^B\right] + \frac{C \, K_2}{1 + \frac{D}{Re \, K_1 \, K_2}} \tag{19}$$

The expression is valid if $(Re \, K_1 \, K_2) < 10^5$. Shape factors K_1 and K_2 are functions of the sphericity and the projected area in the direction of motion. The expressions to derive values for K_1, K_1, A, B, C and D, obtained from the fitting to experimental values, are given elsewhere (Bagheri and Bonadonna, 2016; Ganser, 1993). Dioguardi and Mele and Dioguardi et al. studied the settling of volcanic ash in water by using the ratio between sphericity and circularity in the direction of motion as particle shape factor (Dioguardi and Mele, 2015; Dioguardi et al., 2018). Song et al. developed a model that included the ratio between the surface of the equivalent and the projected area in a plane perpendicular to the settling direction (Song et al., 2017). Wang et al. proposed an expression for cuboids based on several experimental fitting parameters (Wang et al., 2011). It is important to note that all correlations use parameters fitted with experimental values obtained from a given set or particles and their generalization to other shapes may lead to important errors (Loth, 2008).

Tran-Cong et al. performed laboratory measurements aimed at determining the terminal velocity of irregularly shaped agglomerates, including isometric, axisymmetric, orthotropic, and plane and elongated conglomerates of spheres. They developed an empirical correlation for c_D using the ratio of the surface and volume equivalent spheres (d_s/d_v) and particle circularity (c, defined below, in Eq. 34) for the area projected in the direction of motion (Tran-Cong et al., 2004). The expression, tested for 0.15 < Re < 1500, 0.80 < d_s/d_v < 1.50 and 0.4 < c < 1.0 is as follows:

$$c_D = \frac{24}{Re}\frac{d_s}{d_v}\left[1+\frac{0.15}{\sqrt{c}}\left(\frac{d_s}{d_v}Re\right)^{0.687}\right]+ \frac{0.42\left(\frac{d_s}{d_v}\right)^2}{\sqrt{c}\left[1+42500\left(\frac{d_s}{d_v}Re\right)^{-1.16}\right]} \quad (20)$$

Waldschlager and Schüttrumpf specifically studied the behaviour of plastic particles in water and developed separated empirical expressions for settling and buoyant plastics, and for fibres and particles. The characteristic dimension was different for both cases: the diameter in the case of fibres, and the geometric average of the three main dimensions for fragments (Waldschläger and Schüttrumpf, 2019). For buoyant particles and fibres, the following expressions were proposed in which R_P is Power's roundness in a 0-6 scale, computed as shown elsewhere (Powers, 1953):

$$c_{D-fragments} = \left(\frac{20}{Re}+\frac{10}{Re^{1/2}}+\sqrt{1.195-csf}\right)\left(\frac{6}{R_p}\right)^{csf-1} \quad (21)$$

$$c_{D-fibres} = \left(\frac{10}{Re^{1/2}}+\sqrt{csf}\right) \quad (22)$$

While for settling particles and fibres, the drag coefficient was:

$$c_{D-fragments} = \left(\frac{3}{csf\,Re^{1/3}}\right) \quad (23)$$

$$c_{D-fibres} = \left(\frac{4.7}{Re^{1/2}}+\sqrt{csf}\right) \quad (24)$$

For particles of density 1.3 g cm^{-3}, representative for the average density of commercial polymers, Stoke's regime (Re < 0.1) only stands for particles with < 40 µm in air and < 65 µm in water at ambient conditions. Outside the Stoke's regime, the procedure for determining the terminal settling velocity, v_∞, of spherical particles requires the use of an iterative procedure because c_D is a function of Re, which in turn is a function of v_∞. Some researchers developed expressions to directly derive v_∞ from known variables, but the use of modern computers limited their interest (Haider and Levenspiel, 1989). The above mentioned expressions for c_D have different range of applicability but are not limited to Stoke's regime. Some are valid for turbelent flows even up to wake separation, which takes place at Re about 200 000. The effect of small-scale roughness is to reduce the Re at which turbulent wake separation takes place, but Re in realistic situations concerning MPs are much lower, and generally below 10^3 (as show in Fig. 4).

5. Stokes diameter

Fig. 4 compares the values of c_D obtained for a set of particles recovered from environmental samples, that include marine litter and atmospheric samples. A detailed description of all MPs used in Fig. 4 is presented in Table S1 (SM). The figure shows a general agreement among c_D values calculated using different correlations, except in the case of that of Waldschlager and Schüttrumpf for airborne fibres (MPs 18 to 21), most probably because Eqs. 21-24 were developed for MPs falling (or rising) in water. Other important differences were found for fibres but were minor in the case of fragments, which could be attributed to the different choices for state variables and the diverse set of particles used to derive regression coefficients.

Stoke's diameter, d_{St}, is the diameter of a sphere that has the same density and settling velocity as the particle. Substituting V and S_p in Eq. 13 for the values of a sphere of equivalent diameter d_v, the following expression is obtained for the Stoke's diameter:

$$d_{St} = \frac{3\,c_{D(sphere)}\,\rho_f\,v_\infty^2}{4\,\Delta\rho\,g} \quad (25)$$

In which c_D, denoted as $c_{D(sphere)}$, corresponds to spheric particles. To compute the Stoke's diameter of a non-spherical particle, Eq. 13 (with c_D from Eqs. 14-18, 19, 20, 21-24 or other similar) and Eq. 25 (for the Stoke's equivalent sphere) must be simultaneously solved. The simplest case corresponds to close to isometric particles (ϕ > 0.670) in Stokes's regime, for which c_D is very approximately equal to 24/Re. Therefore, combining Eqs. 13 and 25, Stoke's diameter is as follows:

$$d_{St} = \sqrt{\frac{3\,d_v\,V}{2\,S_p}} \quad (26)$$

(It has to be noted that the characteristic dimension for Re is d_v in Eq. 13 and dSt in Eq. 25). For intermediate (0.1 < Re < 1000) and Newton regimes (1000 < Re < 2 x 10^5) up to the transition to turbulent boundary layer in the upstream side of the sphere, the derivation of d_{St} requires an iterative procedure (although straightforward).

Fig. 5 (A and B) shows a comparison between d_v and d_{St} for the set of 21 MPs recovered from marine litter and from atmospheric samples listed in Table S1 (SM). Shape factors based on the main orthogonal dimensions are given in the triangular plot on the left side of Fig. 5A. Stoke's diameter in Fig. 5B was computed using Eq. 25 with $c_{D(sphere)}$ from Eq. 14. Fig. 5 (C and D) displays shape factors for the 140 particles

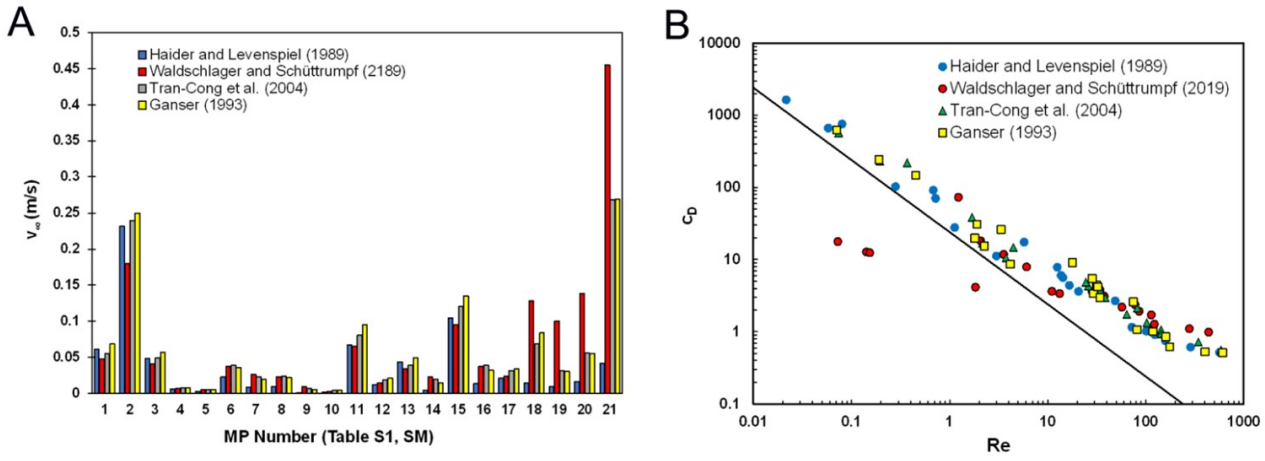

Figure 4: *Values of settling (or rising) velocities predicted by four different models applied to the set of 21 MPs indicated in Table S1(A); values predicted for the drag coefficient, c_D, as a function of Re (B). (The solid line in panel B corresponds to 24/Re.)*

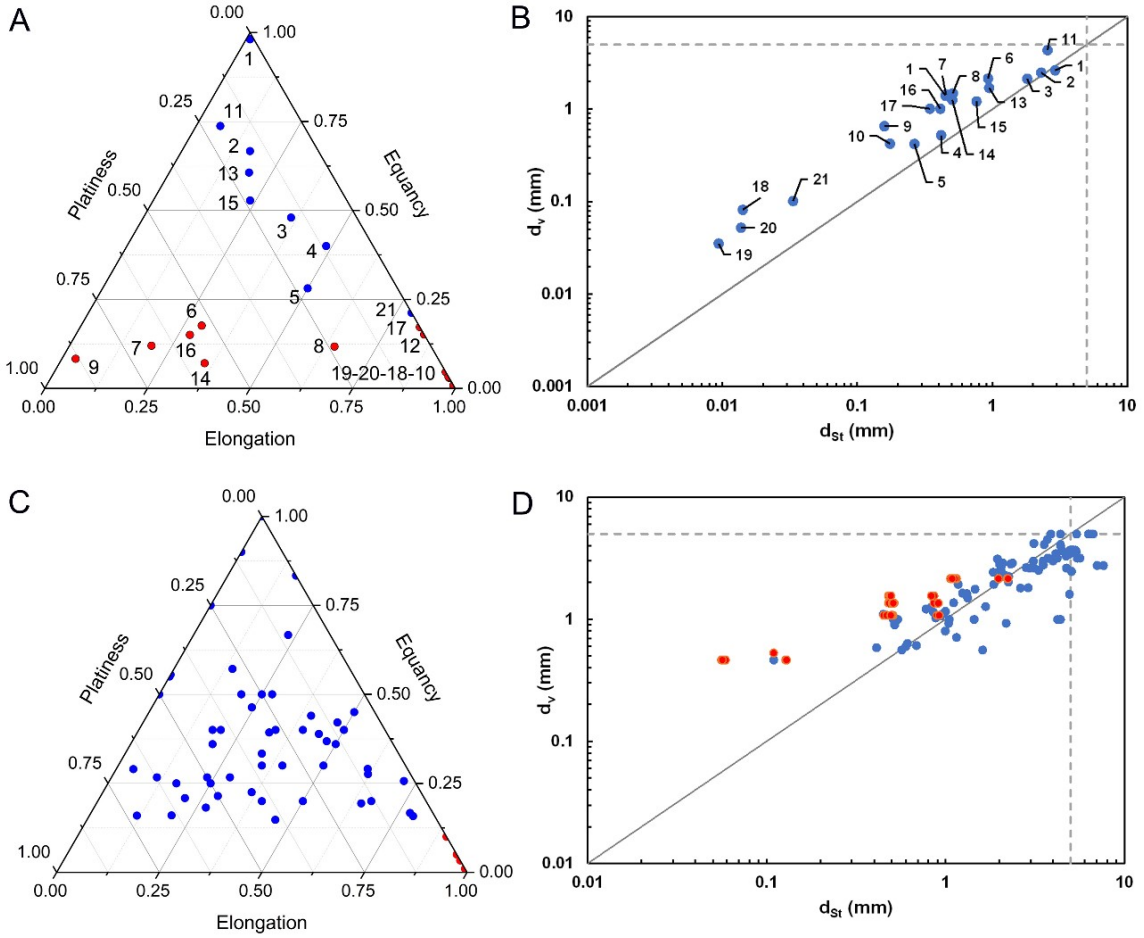

Figure 5: *Equancy, platiness and elongation for MPs found in environmental samples (A). Values of d_v and d_{St} computed from measurements of the three main orthognal dimensions; the points marked in red in A correspond to deviations > 100 % between d_v and d_{St}. (Details for the MPs are provided in Table S1, SM.). Shape factors for the set of 140 fibres, pellets and fragments used by Waldschlager and Schüttrumpf (2019) and computed form the values of d_1, d_2, and d_3 provided by the authors (C). Values of d_v and d_{St} computed using Eqs. 21-25 for the same set of MPs; the points marked in red correspond to fibres (D).*

(48 fibres and 92 pellets and fragments with different shapes) used by Waldschlager and Schüttrumpf (2019). Fibres, marked as red circles in Fig. 5C, display elongation values close to unity because AR_{2D} > 10 in all cases. The calculation of Stoke's diameter was based on the experimental values for settling (or

rising) velocity in water and was computed using Eq. 25 with cD(sphere) obtained from Equations 21-24, which were developed by Waldschlager and Schüttrumpf using the same set of experimental values. Fig. 5D compares d_{St} with d_v, calculated using Eqs.1 and 10 for irregular shapes and from geometric considerations in the case of simple geometrid bodies (spheres and cylinders). The red points in Fig. 5D correspond to the fibres shown in Fig. 5C. The results showed that the differences between dv and dSt can be high for non-isometric shapes, particularly for films and fibres. This is because the drag force is lower in fibres and plates than in spheric particles with the same volume.

The determination of dynamic diameters depends on the availability of accurate expressions for the drag coefficient, c_D, which may be controversial as most of them were not developed for plastics. A major issue is the need to obtain geometric parameters for non-isometric particles. The difficulty of defining a cross-sectional area in non-spheric particles has been addressed in different ways. Dietrich defined a dimensionless particle size calculated from the diameter of the sphere with to the same volume (Dietrich, 1982). This process was recently used for MPs by Khatmullina and Isachenko who obtained expressions obtained for terminal velocities of plastic particles function of several coefficients fitted using experimental values (Khatmullina and Isachenko, 2017).

For the case of airborne particles, the aerodynamic diameter, d_A, is defined in a similar way as Stoke's diameter. It is the diameter of a sphere with unit (or reference) density, ρ_o, with the same settling velocity as the particle. The relationship between d_A and d_{St} is simple:

$$d_A = d_{St}\sqrt{\frac{\rho}{\rho_o}} \tag{27}$$

where ρ_o is the reference density (1 g cm^{-3}). Several expressions have been developed for the aerodynamic diameter of fibres (Gonda and Abd El Khalik, 1985). The following one was derived theoretically for fibres with random orientation by Harris and Fraser (Harris and Fraser, 1976):

$$d_A = \frac{3\,d}{2}\sqrt{\frac{\frac{\rho}{\rho_o}}{\frac{0.385}{ln(2AR_{2D})-0.5}+\frac{1.230}{ln(2AR_{2D})+0.5}}} \tag{28}$$

AR_{2D} is the aspect ratio calculated from two orthogonal dimensions (length/diameter). When considering only the motion perpendicular to fibre axis, the equivalent diameter is lower because of the higher drag, and Eq. 28 can be simplified to:

$$d_A = \frac{3\,d}{2}\sqrt{\frac{\rho}{\rho_o}\frac{ln(2AR_{2D})+0.5}{2}} \tag{29}$$

Both expressions have been derived using the Stoke's law, and, therefore, are only valid for low Re number. For example, for a PET fibre of 1 mm length and 100 µm width falling in air at ambient conditions, Stoke's diameter is 0.229 mm from Eqs. 13 and 25 and 0.211 mm from Eqs. 27-28, < 8 % difference, which is a very good agreement. In this case Re = 0.013, but for larger particles, for example 3 mm length and 500 µm width, Re = 0.73 > 0.1, and, therefore outside the range of validity of Stoke's regime, the assumption behind Eqs. 28 and 29. In this case, Stoke's diameter is 0.85 mm, 13 % lower than the value computed from Eqs. 27-28, which is still a good approximation, however. The information on the behaviour of plastic fragments and fibres in fluid media are particularly relevant for establishing their fate in the atmospheric compartment to feed the kinematic Lagrangian models that computed the trajectories of airborne particles (González-Pleiter et al., 2021)

6. Geometric parameters from projected images

The morphological characterization of three-dimensional particles is a very complex task that requires extensive use of image processing routines and specialized equipment. In many cases, however, the only information available is limited to 2D images obtained from optical or electron microscopes. The way of dealing with projected images is different if multiple images can be taken for every single particle or not. Although some techniques allow capturing images on one of more random planes, in most cases, 2D images represent a single projection of the true 3D shape of the particles over a stable position on a flat surface. The information in this case, could be biased, because the missing information generally corresponds to the shortest particle dimension, making it difficult to obtain accurate shape descriptors.

The main difficulty is to obtain a representative length dimension comparable to the diameter of the sphere with the same volume as the particle. Martin's and Feret's diameter are usually used for obtaining a simple measure of particle size when processing 2D images. Martin's diameter is the distance between opposite sides of the projected image of the particle. Feret's diameter is the distance between parallel tangents on opposite sides of particle's outline (Merkus, 2009). In both cases, more representative values can be obtaining by averaging several individual values.

Another widely used equivalent diameter is that of the circle with the same projected area, d_c:

$$d_c = \left(\frac{4\,S_p}{\pi}\right)^{1/2} \tag{30}$$

Martin's and Feret's diameters and the projected area diameter can be readily obtained from projected images as indicated in Fig. 6. Projected 2D images can be reconstructed by Fourier analyses to obtain the 2D size descriptors, which can be further related to their corresponding 3D size descriptors obtained, for example, from mCT. Accordingly, the two principal 2D dimensions, $d_{1,2D}$ and $d_{2,2D}$, can also be obtained from projected images and, therefore, a 2D size can be defined as follows:

$$d_{2D} = \frac{d_{1,2D} + d_{2,2D}}{2} \tag{31}$$

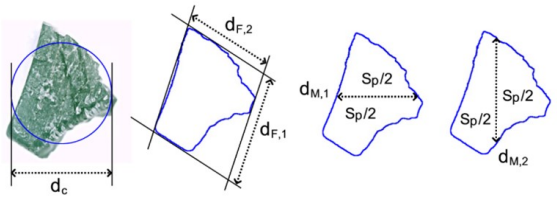

Figure 6: *Equivalent circle diameter, d_c, and Martin's and Feret's diameters from the projected image of a MP particle. $S_p/2$ represent the segment dividing the projected are in two equal parts. There are many Feret's and Martin's diameters even for the same projected image that distribute around a central value.*

The information required to compute dynamic diameters is difficult to obtain using projected images. Particle volume can be calculated for particles with cylindrical symmetry (like fibres) because the intermediate and shortest dimension are equal or very similar, and, therefore, $d_{1,3D} = d_{1,2D}$ and $d_{2,3D} = d_{3,3D} = d_{2,2D}$. For close to isometric particles, there are other possibilities. Using mCT data, it has been shown that 3D larger and shorter principal dimensions, d_1 and d_3, deviate < 10 % from their 2D counterparts, namely $d_{1,2D}$ and $d_{2,2D}$ (Su and Yan, 2020). Besides, the same authors showed that in particles of sufficiently high sphericity $d_{av,2D} \simeq d_{av,3D}$. With that information and assuming ellipsoidal shape, Eqs. 1 and 10, yield the following approximate expression for d_v:

$$d_v \backsimeq \sqrt[3]{(d_{1,2D}\,d_{2,2D})}\,\frac{d_{1,2D} + d_{2,2D}}{2} \tag{32}$$

The values for d_v obtained from Eq. 32 can be compared with Eq. 10 computed with the data from virtual particles created using a 3D particle generator (Cruz-Matías et al., 2019; Lin and Miller, 2005; Maroof et al., 2020). The values calculated for dv show important differences (> 50 %) only for some particles with low sphericity (ϕ < 0.670). The comparison is shown in Fig. 7. for the three sets of particles used in those papers. The results indicated that reasonable dv values can be obtained for nearly isometric particles. The discrepant ones are marked by empty circles in the right panel of Fig. 7. The sphericities for the same outliers are indicated in the left panel.

ImageJ and similar programs also allow computing particle surface and perimeter from projected images. Surface area and perimeter can be used to calculate circularity. The circularity of a projected particle is the degree to which the particle is similar to a circle and according to ISO9276-6 is defined as:

$$C = \sqrt{\frac{4\,\pi\,S_p}{P^2}} \tag{33}$$

In which P is the perimeter of the particle projection. However, it is not circularity, but the circularity index c, or Cox's circularity the magnitude that can be used as 2D proxy for the true sphericity (Cox, 1927; Cruz-Matías et al., 2019):

$$c = C^2 \tag{34}$$

Fig. 6 also shows the comparison between c and ϕ for a set of 3D particles is a reasonable assumption, although sphericities higher than the unity may eventually arise from the information obtained from 2D image analysis. It is important to note that shape parameters may significantly change with particle orientation. If 2D data from several orientations can be obtained, the average of Martin's and Feret's diameters or that of equivalent circle diameters may be taken as an approximation for d_v and the same for circularity index for sphericity (Blott and Pye, 2008). Incidentally, it has been shown that circularity measured form the maximum area projection yielded sphericities with differences generally < 10 % with respect to true sphericity (Bagheri et al., 2015).

Clearly, the information from 2D images leads to better estimations if multiple images from the same particle are available, but this is not the case in most environmental studies of MPs. An important issue is that 2D images provide projected area calculated from a stable position on a flat surface. This surface is not generally the same as that required to compute dynamic diameters using Eq. 12, although the same notation, S_p, was used for both cases. If projected surface cannot be averaged over several projections, a correction factor can be applied that corresponds to the ratio between mean projected area and the projected area of the most stable position. For example, for rod-shape particles ($d_1 > d_2 = d_3$), the stable projected area is d_1 x d_2 and the area averaged over all possible views is:

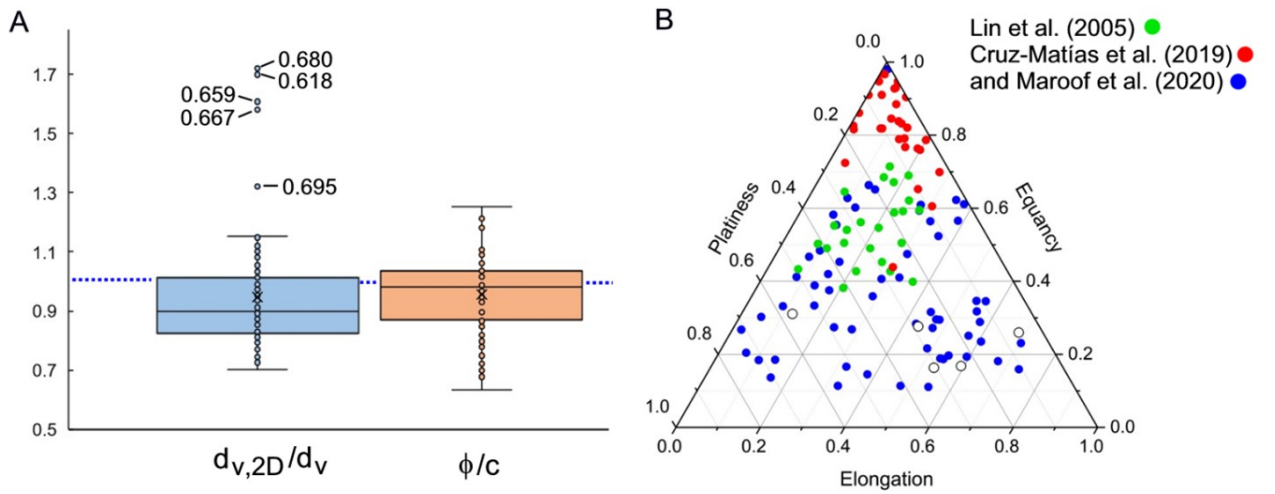

Figure 7: *A: ratio $d_{v,2D}/d_v$ and ϕ/c specifying outliers for the particles described by Lin and Miller (2005, ●), Cruz-Matías et al. (2019, ●), and Maroof et al. (2020, ●). ($d_{v,2D}$ has been calculated using Eq. 31 and c is the circularity index defined below in Eq. 33; the dotted line corresponds to the unity.). B: ternary plot for the same particles displaying the outliers shown in A as empty circles.*

$$\frac{\pi\, d_2^2}{8} + \frac{\pi\, d_1\, d_2}{4}$$

Therefore, the following correction factor (average area/stable projected area) could be applied to convert S_p into its averaged value:

$$\left(\frac{\pi\, d_2^2}{8} + \frac{\pi\, d_1\, d_2}{4}\right)\left(\frac{1}{d_1\, d_2}\right) = \frac{\pi}{8}\left(2 + \frac{d_2}{d_1}\right)$$

Similar expressions for the mean projected area and the projected area of the most stable position in ellipsoids and flat particles can be found elsewhere (Vickers and Brown, 2001). Some additional information on particle geometric can be obtained considering the relationship that exists between the projected area of a particle and its true surface. This is an old problem with a solution outlined by Cauchy in the XIX century and formally proved by Vouk (Vouk, 1948). Cauchy-Vouk's theorem establishes that the surface of a convex (3D) body is the average of all its 2D projections:

$$S = 4\,\bar{S}_p \tag{35}$$

Where $\bar{S}_p$ represents the averaged projected surface considering all possible orientations. Obviously most plastic fragments would not be strictly convex, but Eq. 35 can still be used as an approximation. Comparing 2D and 3D (X-ray-mCT) particle descriptors, Su and Yan obtained satisfactory reconstruction of 3D size and shape using several tens of projections (Su and Yan, 2020). Of course, the number would depend on the error assumed as well as on the exact shape of the particle. Table 2 summarizes the type of information than can be derived depending on the available data on particle geometry and the equations that can be used for it.

7. Conclusions

The morphological description of plastic particles requires a formalized approach that makes easy to compare data from different sources with a minimum degree of subjectivity. A description based on the three main orthogonal dimensions defined as the lengths of the smallest enclosing orthogonal parallelepiped is proposed. Three descriptors, namely equancy, platiness and elongation can define any particle shape and can be easily represented in a ternary plot with the basic 3D (sphere), 2D (plate) and 1D (rod) morphologies as vertexes.

Dynamic or Stoke's diameter representing the settling or buoyancy behaviour of plastic particles in fluid media require data from particle volume, sphericity and surface projected in a plane perpendicular to the motion direction. If 3D morphological descriptors are available, such as the main orthogonal dimensions of the particle, volume can be approximated by an ellipsoid and reasonable assumptions can be made to derive other geometrical descriptors. The results showed that there is a large difference between Stoke's diameter and the diameter of the sphere with the same volume, which is > 100 % for particles with equancy < 0.20 that correspond to non-isometric particles with low sphericity. These particles correspond to fibres or platelike particles, which behave very differently from spherical shapes in fluid media. There is a strong need to develop correlations for irregular particles, especially for airborne fibres.

Table 2. *Information that can be derived from particle size and shape measurements.*

Data available or that can be directly derived	Calculations with moderate assumptions	Calculations with controversial assumptions
Full 3D description		
V s d_v ϕ	S_p (Eq. 35) d_{St} (Eq. 25)	
Projected images obtained from several random positions		
d_1, d_2, d_3 (average) S_p (average) P (average)	V (Eq. 1) S (Eq. 5 or 35) d_v (Eq. 10) ϕ from V and S (Eq. 11), from d_1, d_2 and d_3 (Eq. 4) or from the average of circularity indexes (Eq. 34)	d_{St} (Eqs. 13-21 or 22)
Projected surface from particles lying on stable positions		
$d_{1,2D}$, $d_{2,2D}$ S_p (stable position) P (stable position)	V for particles with cylindrical symmetry (assuming length = $d_{1,2D}$ and width $d_{2,2D}$)	S_p from a single stable position can be used in Eq. 13, possibly using shape correction (Section 6) ϕ from a single circularity index (Eq. 34) d_v from Eq. 32 if particles are close to isometric V from Eq. 10 if particles are close to isometric d_{St} derived using Eqs. 13 and 25 or 26 (except flat particles for which the information on the smaller dimension is lost)

The characterization of plastic-fluid interaction is difficult in the absence of three-dimensional shape descriptors. The use of microtomography instrumentation would be of great help. Having available only projected images, the derivation of dynamic diameters, and other size descriptors, can be performed, but the approximations are poor in the case of non-isometric particles.

Acknowledgements

The author acknowledges the support provided by the Thematic Network of Micro- and Nanoplastics in the Environment, EnviroPlaNet Network (RED2018-102345-T).

Notation

AR_{2D} = aspect ratio calculated from two orthogonal dimensions (-)
AR_{3D} = aspect ratio calculated from three orthogonal dimensions [Eq. 3] (-)
C = circularity [Eq. 33] (-)
c = circularity index [Eq. 34] (-)
csf = Corey's shape factor [Eq. 4] (-)
c_D = drag coefficient [Eq. 12] (-)
d = diameter of a spheric or cylindric particle (m)
d_1, d_2, d_3 = main orthogonal dimensions (m)
d_{2D} = mean size based on two dimensions of a projected image (m)
d_{3D} = mean size based on three orthogonal dimensions [Eq. 2] (m)
d_A = aerodynamic diameter [Eq. 28] (m)
d_c = diameter of the circle with the same projected area [Eq. 30] (m)
d_{St} = Stoke's diameter of a particle [Eq. 25] (m)
d_v = diameter of the sphere with the same volume [Eq. 10] (m)
d_s = diameter of the sphere with the same surface (m)
F_D = drag force [Eq. 12] (N)
P = perimeter of a particle projection (m)
R_P = Power's roundness [Eq. 21] (-)
Re = Reynolds number ($d\, v_\infty\, \rho_f\, \mu_f^{-1}$)
S = surface of a particle (m^2)

S_p = projected area (m^2)
$\bar{S}_p$ = average projected area considering all possible orientations (m^2)
v_∞ = settling velocity (m s^{-1})
V = volume of a particle (m^3)
ϕ = sphericity [Eq. 11] (-)
μ = fluid viscosity (Pa s)
ρ_f = fluid density (kg m^{-3})
ρ_p = particle density (kg m^{-3})
ρ_o = reference density (1 g cm^{-3} or 1000 kg m^{-3})

References

Bagheri, G., Bonadonna, C., 2016. On the drag of freely falling non-spherical particles. Powder Technol. 301, 526-544. Bagheri, G.H., Bonadonna, C., Manzella, I., Vonlanthen, P., 2015. On the characterization of size and shape of irregular particles. Powder Technol. 270, 141-153.

Besseling, E., Quik, J.T.K., Sun, M., Koelmans, A.A., 2017. Fate of nano- and microplastic in freshwater systems: A modeling study. Environ. Pollut. 220, 540-548.

Blott, S.J., Pye, K., 2008. Particle shape: a review and new methods of characterization and classification. Sedimentology 55, 31-63.

Bozzini, B., Altissimo, M., Amati, M., Bocchetta, P., Gianoncelli, A., Gregoratti, L., Kourousias, G., Mancini, L., Mele, C., Kiskinova, M., 2018. In situ and ex situ X-ray microspectroelectrochemical methods for the study of zinc–air batteries, in: Wandelt, K. (Ed.), Encyclopedia of Interfacial Chemistry. Elsevier, Oxford, pp. 174-194.

Brandt, J., Bittrich, L., Fischer, F., Kanaki, E., Tagg, A., Lenz, R., Labrenz, M., Brandes, E., Fischer, D., Eichhorn, K.J., 2020. High-throughput analyses of microplastic samples using fourier transform infrared and raman spectrometry. Appl. Spectrosc. 74, 1185-1197.

Burns, E.E., Boxall, A.B.A., 2018. Microplastics in the aquatic environment: Evidence for or against adverse impacts and major knowledge gaps. Environ. Toxicol. Chem. 37, 2776-2796.

Clift, R., Gauvin, W.H., 1971. Motion of entrained particles in gas streams. Can. J. Chem. Eng. 49, 439-448.

Cowger, W., Gray, A., Christiansen, S.H., DeFrond, H., Deshpande, A.D., Hemabessiere, L., Lee, E., Mill, L., Munno, K., Ossmann, B.E., Pittroff, M., Rochman, C., Sarau, C., Tarby, S., Primpke, S., 2020. Critical review of processing and classification techniques for images and spectra in microplastic research. Appl. Spectrosc. 74, 989-1010.

Cox, E.P., 1927. A method of assigning numerical and percentage values to the degree of roundness of sand grains. J. Paleontol. 1, 179-183.

Cruz-Matías, I., Ayala, D., Hiller, D., Gutsch, S., Zacharias, M., Estradé, S., Peiró, F., 2019. Sphericity and roundness computation for particles using the extreme vertices model. J. Comput. Sci. 30, 28-40.

Dietrich, W.E., 1982. Settling velocity of natural particles. Water Resour. Res. 18, 1615-1626.

Dioguardi, F., Mele, D., 2015. A new shape dependent drag correlation formula for non-spherical rough particles. Experiments and results. Powder Technol. 277, 222-230.

Dioguardi, F., Mele, D., Dellino, P., 2018. A new one-equation model of fluid drag for irregularly shaped particles valid over a wide range of Reynolds number. Journal of Geophysical Research: Solid Earth 123, 144-156.

ECHA, 2020. Background Document to the Opinion on the Annex XV report proposing restrictions on intentionally added microplastics, ECHA/RAC/RES-O-0000006790-71-01/F and ECHA/SEAC/RES-O-0000006901-74-01/F. European Chemicals Agency, Helsinki.

Edo, C., Fernández-Alba, A.R., Vejsnæs, F., van der Steen, J.J.M., Fernández-Piñas, F., Rosal, R., 2021. Honeybees as active samplers for microplastics. Sci. Total Environ. 767, 144481.

Edo, C., Tamayo-Belda, M., Martínez-Campos, S., Martín-Betancor, K., González-Pleiter, M., Pulido-Reyes, G., García-Ruiz, C., Zapata, F., Leganés, F., Fernández-Piñas, F., Rosal, R., 2019. Occurrence and identification of microplastics along a beach in the Biosphere Reserve of Lanzarote. Mar. Pollut. Bull. 143, 220-227.

Forsberg, P.L., Sous, D., Stocchino, A., Chemin, R., 2020. Behaviour of plastic litter in nearshore waters: First insights from wind and wave laboratory experiments. Mar. Pollut. Bull. 153, 111023.

Frias, J., Pagter, E., Nash, R., O'Connor, I., Carretero, O., Filgueiras, A., Viñas, L., Gago, J., Antunes, J., Bessa, F., Sobral, P., Goruppi, A., Tirelli, V., Pedrotti, M.L., Suaria, G., Aliani, S., Lopes, C., Raimundo, J., Caetano, M., Gerdts, G., 2018. Standardised protocol for monitoring microplastics in sediments. JPI-Oceans BASEMAN project Deliverable D4.2.

Frias, J.P.G.L., Nash, R., 2019. Microplastics: Finding a consensus on the definition. Mar. Pollut. Bull. 138, 145-147. Ganser, G.H., 1993. A rational approach to drag prediction of spherical and nonspherical particles. Powder Technol. 77, 143-152.

Garboczi, E.J., Bullard, J.W., 2017. 3D analytical mathematical models of random star-shape particles via a combination of X-ray computed microtomography and spherical harmonic analysis. Advanced Powder Technology 28, 325-339.

GESAMP, 2015. Sources, fate and effects of microplastic in the marine environment: A global assessment, in: Kershaw, P.J. (Ed.). IMO/FAO/UNESCO-IOC/UNIDO/WMO/IAEA/UN/UNEP/UNDP/ISA Joint Group of Experts on the Scientific Aspects of Marine Environmental Protection, p. 220.

GESAMP, 2016. Sources, fate and effects of microplastic in the marine environment: Part two of a global assessment, in: Kershaw, P.J., Rochman, C.M. (Eds.). Joint Group of Experts on the Scientific Aspects of Marine Environmental Protection, p. 220.

GESAMP, 2019. Guidelines for the monitoring and assessment of plastic litter in the ocean, in: Kershaw, P.J., Turra, A., Galgani, F. (Eds.). Joint Group of Experts on the Scientific Aspects of Marine Environmental Protection, p. 130.

Gigault, J., Halle, A.t., Baudrimont, M., Pascal, P.-Y., Gauffre, F., Phi, T.-L., El Hadri, H., Grassl, B., Reynaud, S., 2018. Current opinion: What is a nanoplastic? Environ. Pollut. 235, 1030-1034.

Gonda, I., Abd El Khalik, A.F., 1985. On the calculation of aerodynamic diameters of fibers. Aerosol Sci. Technol. 4, 233-238.

González-Pleiter, M., Edo, C., Aguilera, Á., Viúdez-Moreiras, D., Pulido-Reyes, G., González-Toril, E., Osuna, S., de Diego-Castilla, G., Leganés, F., Fernández-Piñas, F., Rosal, R., 2021. Occurrence and transport of microplastics sampled within and above the planetary boundary layer. Sci. Total Environ. 761, 143213.

Gray, A.D., Weinstein, J.E., 2017. Size- and shape-dependent effects of microplastic particles on adult daggerblade grass shrimp (Palaemonetes pugio). Environ. Toxicol. Chem. 36, 3074-3080.

Haider, A., Levenspiel, O., 1989. Drag coefficient and terminal velocity of spherical and nonspherical particles. Powder Technol. 58, 63-70.

Happel, J., Brenner, H., 2012. Low Reynolds number hydrodynamics: with special applications to particulate media. Springer Science and Business Media (p, 42).

Harris, R.L., Fraser, D.A., 1976. A model for deposition of fibers in the human respiratory system. Am. Ind. Hyg. Assoc. J. 37, 73-89.

Hartmann, N.B., Hüffer, T., Thompson, R.C., Hassellöv, M., Verschoor, A., Daugaard, A.E., Rist, S., Karlsson, T., Brennholt, N., Cole, M., Herrling, M.P., Hess, M.C., Ivleva, N.P., Lusher, A.L., Wagner, M., 2019. Are we speaking the same language? Recommendations for a definition and categorization framework for plastic debris. Environ. Sci. Technol. 53, 1039-1047.

Hidalgo-Ruz, V., Gutow, L., Thompson, R.C., Thiel, M., 2012. Microplastics in the marine environment: A review of the methods used for identification and quantification. Environ. Sci. Technol. 46, 3060-3075.

Keller, S.R., 1979. On the surface area of the ellipsoid. Math. Comput. 33, 310-314. Khatmullina, L., Isachenko, I., 2017. Settling velocity of microplastic particles of regular shapes. Mar. Pollut. Bull. 114, 871-880.

Kowalski, N., Reichardt, A.M., Waniek, J.J., 2016. Sinking rates of microplastics and potential implications of their alteration by physical, biological, and chemical factors. Mar. Pollut. Bull. 109, 310-319.

LaGrone, J., Cortez, R., Yan, W., Fauci, L., 2019. Complex dynamics of long, flexible fibers in shear. J. Non-Newtonian Fluid Mech. 269, 73-81.

Lin, C.L., Miller, J.D., 2005. 3D characterization and analysis of particle shape using X-ray microtomography (XMT). Powder Technol. 154, 61-69.

Loth, E., 2008. Drag of non-spherical solid particles of regular and irregular shape. Powder Technol. 182, 342-353. Lusher, A.L., Bråte, I.L.N., Munno, K., Hurley, R.R., Welden, N.A., 2020. Is it or isn't it: the importance of visual classification in microplastic characterization. Appl. Spectrosc. 74, 1139-1153.

Magni, S., Binelli, A., Pittura, L., Avio, C.G., Della Torre, C., Parenti, C.C., Gorbi, S., Regoli, F., 2019. The fate of microplastics in an Italian Wastewater Treatment Plant. Sci. Total Environ. 652, 602-610.

Maroof, M.A., Mahboubi, A., Noorzad, A., Safi, Y., 2020. A new approach to particle shape classification of granular materials. Transp. Geotech. 22, 100296.

Merikallio, S., Muñoz, O., Sundström, A.-M., Virtanen, T.H., Horttanainen, M., Leeuw, G.d., Nousiainen, T., 2015. Optical modeling of volcanic ash particles using ellipsoids. J. Geophys. Res.: Atmos. 120, 4102-4116.

Merkus, H.G., 2009. Particle Size Measurements: Fundamentals, Practice, Quality. Springer Science. Obbard, R.W., 2018. Microplastics in Polar Regions: The role of long range transport. Curr. Opin. Environ. Sci. Health 1, 24-29.

Powers, M.C., 1953. A new roundness scale for sedimentary particles. J. Sediment. Res. 23, 117-119.

Rivers, M.L., Gwinnett, C., Woodall, L.C., 2019. Quantification is more than counting: Actions

required to accurately quantify and report isolated marine microplastics. Mar. Pollut. Bull. 139, 100-104.

Safonov, I., Yakimchuk, I., Abashkin, V., 2018. Algorithms for 3D particles characterization using X-ray microtomography in proppant crush test. Journal of Imaging 4, 134.

Sagawa, N., Kawaai, K., Hinata, H., 2018. Abundance and size of microplastics in a coastal sea: Comparison among bottom sediment, beach sediment, and surface water. Mar. Pollut. Bull. 133, 532-542.

Semcesen, P.O., Wells, M.G., 2021. Biofilm growth on buoyant microplastics leads to changes in settling rates: Implications for microplastic retention in the Great Lakes. Mar. Pollut. Bull. 170, 112573.

Song, X., Xu, Z., Li, G., Pang, Z., Zhu, Z., 2017. A new model for predicting drag coefficient and settling velocity of spherical and non-spherical particle in Newtonian fluid. Powder Technol. 321, 242-250.

Su, D., Yan, W.M., 2020. Prediction of 3D size and shape descriptors of irregular granular particles from projected 2D images. Acta Geotech. 15, 1533-1555.

Szabó, T., Domokos, G., 2010. A new classification system for pebble and crystal shapes based on static equilibrium points. Central European Geology 53, 1-19.

Tötzke, C., Oswald, S.E., Hilger, A., Kardjilov, N., 2021. Non-invasive detection and localization of microplastic particles in a sandy sediment by complementary neutron and X-ray tomography. J. Soils Sediments 21, 1476-1487.

Tran-Cong, S., Gay, M., Michaelides, E.E., 2004. Drag coefficients of irregularly shaped particles. Powder Technol. 139, 21-32.

Ulanovsky, A., Pröhl, G., 2006. A practical method for assessment of dose conversion coefficients for aquatic biota. Radiat. Environ. Biophys. 45, 203-214.

Vickers, G.T., Brown, D.J., 2001. The distribution of projected area and perimeter of convex, solid particles. Proceedings of the Royal Society of London, Series A 457, 283-306.

Vighi, M., Bayo, J., Fernández-Piñas, F., Gago, J., Gómez, M., Hernández-Borges, J., Herrera, A., Landaburu, J., Muniategui-Lorenzo, S., Muñoz, A.R., Rico, A., Romera-Castillo, C., Viñas, L., Rosal, R., 2021. Micro and nano-plastics in the environment: Research priorities for the near future. Rev. Environ. Contam. Toxicol. in press.

Vouk, V., 1948. Projected area of convex bodies. Nature 162, 330-331.

Waldschläger, K., Schüttrumpf, H., 2019. Effects of particle properties on the settling and rise velocities of microplastics in freshwater under laboratory conditions. Environ. Sci. Technol. 53, 1958-1966.

Wang, J., Qi, H., Zhu, J., 2011. Experimental study of settling and drag on cuboids with square base. Particuology 9, 298-305.

Wang, W., Ge, J., Yu, X., Li, H., 2020. Environmental fate and impacts of microplastics in soil ecosystems: Progress and perspective. Sci. Total Environ. 708, 134841.

Supplementary Materials

Morphological description of microplastic particles for environmental fate studies

Roberto Rosal*

Department of Chemical Engineering, Universidad de Alcalá, E-28871 Alcalá de Henares, Madrid, Spain

* Corresponding author: oberto.rosal@uah.es

Table S1. *MPs used in this study.*

No.	Description	Origin	d_1 (mm)	d_2 (mm)	d_3 (mm)	S (mm^2)	P (mm)
1	PE Yellow Sphere	Marine	2.7	2.6	2.6	5.5	8.3
2	PS White Foam	Marine	3.0	2.5	2.0	5.6	8.4
3	PP Green Fragment	Marine	3.2	2.0	1.5	4.9	9.6
4	PE Green Fragment	Marine	0.89	0.46	0.35	0.32	3.0
5	PE Yellow Fragment	Marine	0.81	0.41	0.23	0.31	2.7
6	PP Blue Plate	Marine	4.3	3.0	0.76	8.2	13.6
7	PP Purple Slab	Marine	3.2	2.5	0.38	5.9	12.0
8	Rubber Red Plate	Marine	4.3	1.5	0.51	6.7	14.4
9	PE White Plate	Marine	1.5	1.5	0.13	2.4	6.3
10	PP Green Fibre	Marine	3.3	0.15		0.43	7.0
11	PE Fragment	Marine	4.9	4.6	3.6	25.4	19.7
12	PE Filament	Marine	5.0	0.75		3.7	12.1
13	PP Fragment	Marine	2.2	1.7	1.3	2.7	7.9
14	PP Film	Marine	3.5	2.3	0.25	6.3	9.8
15	PS Foam	Marine	1.7	1.3	0.87	1.9	5.5
16	PVC Plate	Marine	2.1	1.5	0.32	3.1	7.3
17	Polyester Fibre	Marine	3.7	0.56		1.8	7.5
18	PA Fibre	Airborne	2.0	0.017		0.033	4.0
19	Viscose Fibre	Airborne	0.37	0.011		0.0040	0.75
20	Polyester) Fibre	Airborne	0.51	0.017		0.0086	1.1
21	Polyester) Fibre	Airborne	0.28	0.061		0.065	1.1

Origin of particles: Sampling in Rodeira Beach, Cangas (Pontevedra, Spain) and the following references: Edo, C.,

Tamayo-Belda, M., Martínez-Campos, S., Martín-Betancor, K., González-Pleiter, M., Pulido-Reyes, G., García-Ruiz, C., Zapata, F., Leganés, F., Fernández-Piñas, F., Rosal, R., 2019. Occurrence and identification of microplastics along a beach in the Biosphere Reserve of Lanzarote. Mar. Pollut. Bull. 143, 220-227 González-Pleiter, M., Edo, C., Aguilera, Á.,

Viúdez-Moreiras, D., Pulido-Reyes, G., González-Toril, E., Osuna, S., de Diego-Castilla, G., Leganés, F., Fernández-Piñas, F., Rosal, R., 2021. Occurrence and transport of microplastics sampled within and above the planetary boundary layer. Sci. Total Environ. 761, 143213.